Journal of Materials Science: Materials in Electronics (2019) 30:3804–3810
https://doi.org/10.1007/s10854-019-00664-y

Effects of co-activator species and transition metal ions doping on structure and fluorescence properties of strontium aluminate phosphors

Xiaowu Hu[1,2] · Limin Wu[1] · Hao Yin[1,2] · Guizhi Li[1] · Dongcai Guo[1,2]

Received: 2 September 2018 / Accepted: 2 January 2019 / Published online: 29 January 2019

Abstract
The phosphors of $SrAl_2O_4$: Eu^{2+}, RE^{3+} (RE = Dy^{3+}, Tb^{3+}, Ho^{3+}, La^{3+}, Nd^{3+}, Y^{3+}, Tm^{3+}, Er^{3+}) and $SrAl_2O_4$: Eu^{2+}, Dy^{3+}, M^{2+} (M = Mn^{2+}, Ni^{2+}, Mg^{2+}, Cu^{2+}, Zn^{2+}) were synthesized by co-precipitation combined hydrothermal method, and analyzed by X-ray diffraction (XRD), fluorescence spectrometer and SEM. XRD patterns illustrated that the synthesized products all were the mixed crystal phase of $SrAl_2O_4$ and $Sr_4Al_{14}O_{25}$. The diffraction peaks shapes of phosphors $SrAl_2O_4$: Eu^{2+}, RE^{3+} (RE = Tb^{3+}, Ho^{3+}, Y^{3+}) were almost unchanged contrast to the marked changes of phosphors $SrAl_2O_4$: Eu^{2+}, RE^{3+} (RE = Tm^{3+}, Er^{3+}, Nd^{3+}, La^{3+}), which showed co-activator species had a great impact on the crystal field around the emission center (Eu^{2+}). Besides, the peak positions of $SrAl_2O_4$: Eu^{2+}, Dy^{3+}, M^{2+} (M = Mn^{2+}, Ni^{2+}, Mg^{2+}, Cu^{2+}, Zn^{2+}) were unaltered after doping, while the peak intensity of crystal phase $Sr_4Al_{14}O_{25}$ was enhanced after doped by cations (Mn^{2+}, Ni^{2+}, Cu^{2+}, Zn^{2+}), which indicated the doping of transition metal ions would cause the crystal phase transition. The fluorescence analysis results indicated that the luminescent intensity were reduced after being doped by co-activator ions (Dy^{3+}, Tb^{3+}, Ho^{3+}, La^{3+}, Nd^{3+}, Y^{3+}), but enhanced when doped by co-activator ions (Tm^{3+}, Er^{3+}), and the final emission wavelength and intensity sequence were as follows: $\lambda_{Nd} < \lambda_{La} < \lambda_{Er} < \lambda_{Y} < \lambda_{Tm} < \lambda_{Tb} < \lambda_{Ho} < \lambda_{Dy}$, $I_{Nd} < I_{Dy} < I_{Y} < I_{Tb} < I_{Ho} < I_{La} < I_{Tm} < I_{Er}$. Instead, the fluorescence emission intensity decreased with the increment of the doping concentration of transition metal ions, which perhaps because the transition metal ions doping under the optimal concentration of co-activator could reduce the luminescence intensity of products due to the concentration quenching. The crystal particles of $SrAl_2O_4$: Eu^{2+}, Dy^{3+} presented regular hexagon flake-like morphology with a width of ~ 500 nm and a thickness of ~ 70 nm. The title products could be applied in the safety indicators, emergency lighting danger signals, automobiles, solar cells, etc.

1 Introduction

In recent years, the study fever of inorganic phosphors has been on going, owing to their wide application in safety indicators, solar cells [1], luminescent glass [2], luminescent ceramics [3], luminescent fiber [4], photocatalytic [5], field emission displays [6] and so on. Wherein, rare earth doped alkaline aluminates phosphors are paid much attention for their excellent light stability and afterglow performance, strong chemical stability, no radioactive pollution.

The luminescent properties of alkaline aluminates phosphors are affected by many factors such as matrix, activator, co-activator, etc. The different matrix composition can cause various luminescent colors, such as blue-emitting $CaAl_2O_4$ [7]: Eu^{2+}, Dy^{3+}, green-emitting $BaAl_2O_4$ [8]: Eu^{2+}, Dy^{3+}, blue-green-emitting $Sr_xCa_{(1-x)/2}Ba_{(1-x)/2}Al_2O_4$ [9]: Eu^{2+}, Dy^{3+} and green-emitting $Sr_3Al_2O_6$: Eu^{2+}(Eu^{3+}), Dy^{3+} [10]. In particular, $SrAl_2O_4$: Eu^{2+}, Dy^{3+} as one of the alkaline aluminates phosphors has been studied extensively due to its high luminescent intensity and long-lasting time. The most common activators are rare earth ions (Eu^{2+}, Yb^{2+}, Ce^{3+}, Tm^{2+}, Pr^{3+}, Tm^{2+}, Tb^{3+}), in which Eu^{2+} ion is the main activator due to lower transition level and higher charge transfer energy level. The lower valence activators generally need co-activators to provide electron traps, so trivalent rare earth ions are often used as co-activators to improve the

✉ Dongcai Guo
dcguo2001@hnu.edu.cn

[1] School of Chemistry and Chemical Engineering, Hunan University, Changsha 410082, China

[2] Hunan Provincial Key Laboratory for Cost-effective Utilization of Fossil Fuel Aimed at Reducing Carbon-dioxide Emissions, Changsha 410082, China

luminescence properties of aluminates effectively. Conventional reports suggest the species of co-activators ions have no any effects on the emission wavelength of aluminates phosphors [11], however, they are very important for the study of Eu^{2+} luminescence properties, so they play an very vital role in the research of aluminates phosphors. Up to now, the research of strontium aluminate phosphors mainly focuses on the co-doping of Eu^{2+} and Dy^{3+} ions. There is rare report about the doping of other co-activator ions and transition metal ions, which motivates the present work.

Here, we prepared strontium aluminates phosphors co-doped with Eu^{2+} ion and other cations through combining the hydrothermal and co-precipitation methods, which enables us to successfully obtain homogeneous particles with good crystallinity and high purity. The products were analyzed by means of X ray diffraction (XRD), fluorescence spectrum and scanning electron microscopy (SEM). Further, the details about the effects of transition metal ions (Mn^{2+}, Ni^{2+}, Mg^{2+}, Cu^{2+}, Zn^{2+}) and co-activator ions (Dy^{3+}, Tb^{3+}, Ho^{3+}, Tm^{3+}, Er^{3+}, La^{3+}, Nd^{3+}, Y^{3+}) on the properties of products were investigated.

2 Experiment procedure

2.1 Materials

Europium oxide [Eu_2O_3, 99.99%], dysprosium oxide [Dy_2O_3, 99.99%], terbium oxide [Tb_2O_3, 99.99%], holmium oxide [Ho_2O_3, 99.99%], thulium oxide [Tm_2O_3, 99.99%], erbium oxide [Er_2O_3, 99.99%], lanthanum oxide [La_2O_3, 99.99%], neodymium oxide [Nd_2O_3, 99.99%], yttrium oxide [Y_2O_3, 99.99%], aluminum nitrate [$Al(NO_3)_3{\cdot}9H_2O$ (AR)], nickel nitrate [$Ni(NO_3)_2$ (AR)], manganese nitrate [$Mn(NO_3)_2$ (AR)], cupric nitrate [$Cu(NO_3)_2$ (AR)], zinc nitrate [$Zn(NO_3)_2$ (AR)], magnesium nitrate [$Mg(NO_3)_2$ (AR)], urea [NH_2CONH_2 (AR)], nitric acid [HNO_3 (GR)], polyethylene glycol 200 [$HO(CH_2CH_2O)_nH$ (CP)], boric acid [H_3BO_3 (GR)], granular activated carbon (AR), strontium nitrate [$Sr(NO_3)_2$ (AR)], ammonium carbonate [$(NH_4)_2CO_3$ (AR)], absolute alcohol ($\geq$ 99.7%). All chemical reagents were used as received without further purification.

2.2 Property measurements

X ray diffraction (XRD) analysis: The crystal phase detection of the products was conducted via Shanghai International Trade Co. Ltd XRD-6100 polycrystalline powder X ray analyzer (Cu Kα radiation); tube voltage 40 kV; tube current 30 mA; 2θ angle ranges from 10 to 80 with a step of 0.02 and counting time of 4°/min.

Fluorescence spectrum analysis: The solid fluorescence was measured by HITACHI F-2700 fluorescence spectrometer at room temperature (operation voltage 400 V, with a slit width of 5 nm).

Scanning electron microscope (SEM) analysis: The microscopy of the crystal particles was measured by F20 SEM (model TecnaiG^2 F20 S-TWIN, the United States FEI).

2.3 Synthesis method

The amount of aluminum nitrate (n_{Al}/n_{Sr}) is represented by the molar ratio of aluminum nitrate and strontium nitrate. The amount of activator (n_{Eu}/n_{Sr}) is expressed by the molar ratio of europium nitrate and strontium nitrate. The amount of co-activator ions and transition metal ions (n_{RE}/n_{Eu}, RE = Dy^{3+}, Tb^{3+}, Ho^{3+}, Tm^{3+}, Er^{3+}, La^{3+}, Nd^{3+}, Y^{3+}, n_M/n_{Eu}, M = Mn^{2+}, Ni^{2+}, Mg^{2+}, Cu^{2+}, Zn^{2+},) is shown by the molar ratio of metal nitrate and europium nitrate. The amount of flux is expressed by the mass ratio of solid boric acid and resultant precipitation M_B/M_P.

The products were synthesized under the optimal synthesis conditions via the co-precipitation combined hydrothermal method previously described [12] with some modifications. Firstly, urea (2.24 g) was dissolved in deionized water at room temperature to form homogeneous solution. Next, PEG-200 (4.96 g) was added at 80 °C, followed by $Al(NO_3)_3$ (8 mL) and $Sr(NO_3)_2$ (4 mL) (n_{Al}/n_{Sr} = 2) solution were added in turn and kept stirring. Subsequently, a certain volume of $Eu(NO_3)_3$ (n_{Eu}/n_{Sr} = 0.02) and $Dy(NO_3)_3$ solution (n_{Dy}/n_{Eu} = 2.5) were also added and stirred for 0.5 h to uniform. $(NH_4)_2CO_3$ (over 10%) solution was slowly dropped into the above mixture until the pH value reached 8.5. Then the resultant solution was vigorously stirred for 2 h, transferred to a 100 mL hydro-thermal reactor and treated at 170 °C for 8 h. After the reactor was cooled to room temperature, the resultants were filtered and washed with ethanol and deionized water for 2–3 times respectively, and then put into air dry oven to dry for 24 h, a certain proportion flux (H_3BO_3) (M_B/M_P = 10%) was added after weighing. Finally, the evenly mixed solution was put into the crucible and was calcinated under 1200 °C for 2.5 h in a muffle furnace at a reducing atmosphere provided by activated carbon, and then the product was obtained. The derivatives $SrAl_2O_4$: Eu^{2+}, RE^{3+} and $SrAl_2O_4$: Eu^{2+}, Dy^{3+}, M^{2+} were also prepared by adding the appropriate stoichiometric quantities of transition metal ions and co-activators following the same procedure.

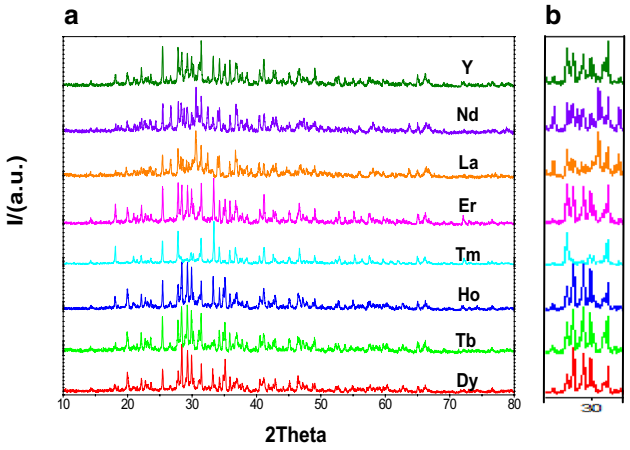

Fig. 1 **a** XRD pattern of $SrAl_2O_4$: Eu^{2+}, RE^{3+} phosphors (RE = Dy, Tb, Ho, Tm, Er, La, Nd, Y, n_{RE}/n_{Eu} = 2.5/1). **b** Magnified XRD patterns from 28° to 32°

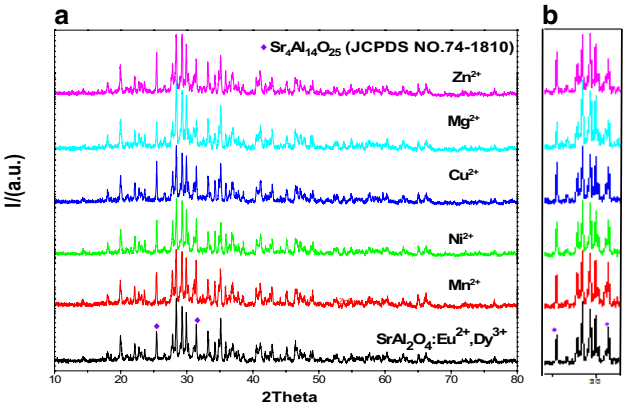

Fig. 2 **a** XRD pattern of $SrAl_2O_4$: Eu^{2+}, Dy^{3+}, M^{2+} phosphors (M = Mn, Ni, Mn, Cu, Zn). **b** Magnified XRD patterns from 24° to 32°

3 Results and discussion

3.1 XRD analysis

3.1.1 XRD analysis of $SrAl_2O_4$: Eu^{2+}, RE^{3+} phosphors

XRD patterns of $SrAl_2O_4$: Eu^{2+}, RE^{3+} phosphors were shown in Fig. 1a. It could be seen that $SrAl_2O_4$: Eu^{2+}, RE^{3+} phosphors presented different diffraction peaks shapes after doped by different co-activator ions. Take the $SrAl_2O_4$: Eu^{2+}, Dy^{3+} as reference, it could be seen clearly from the Fig. 1b that the diffraction peaks shapes were not changed obviously when co-activator ions were Ho (104.1 pm), Tb (106.3 pm), Y (104 pm), because they are about the same radius with Dy^{3+} ion (105.2 pm). Nevertheless, the peaks shapes were altered when co-activator ions were Tm (102.0 pm), Er (103.0 pm), Nd (112.3 pm), La (117.2 pm), due to the large gap of them between Dy^{3+} ions. The matrix lattice distortion occurred in varied degrees when the co-activator ions with different radius were doped into matrix lattice. Hence, it could be concluded that the species of co-activator ions had a great impact on the crystal field around the emission center (Eu^{2+}).

3.1.2 XRD analysis of $SrAl_2O_4$: Eu^{2+}, Dy^{3+}, M^{2+} phosphors

XRD pattern of $SrAl_2O_4$: Eu^{2+}, Dy^{3+}, M^{2+} phosphors were shown in Fig. 2a. Here, $SrAl_2O_4$: Eu^{2+}, Dy^{3+} was chosen as the target of doping owing to its extensive research. It could be observed that all products consisted of main crystal phase $SrAl_2O_4$ (JCPDS NO.34–0379) and a part of hybrid phase $Sr_4Al_{14}O_{25}$ (JCPDS NO.74-1810), and showed high intensity and a strong sharpness, which indicated high crystallization degree of products. Besides, we could see from the Fig. 2b that the XRD peak positions of products were not changed significantly under different transition metal ions doping, however, the intensity of the diffraction peak of $Sr_4Al_{l4}O_{25}$ was reinforced after the doping of Mn^{2+}, Ni^{2+}, Cu^{2+}, Zn^{2+} ions and decreased after the doping of Mg^{2+} ion. The possible reason was that the atomic mass of Mg^{2+} ion (24.31) is much smaller than Sr^{2+} ion (87.62). Accordingly, it could be deduced that the doping of transition metal ions may cause the crystal phase transition of main crystal phase toward hybrid phase, and thus the crystal field around the emission center (Eu^{2+}) to be changed.

3.2 Fluorescence spectrum analysis

3.2.1 Fluorescence spectrum analysis of $SrAl_2O_4$: Eu^{2+}, RE^{3+} phosphors

It was shown from Fig. 3 that the species of co-activators ions had a great impact on emission wavelength and fluorescent emission intensity of products. The sequences of emission wavelength and fluorescence intensity were as follows: $\lambda_{Nd} < \lambda_{La} < \lambda_Y < \lambda_{Tm} < \lambda_{Er} < \lambda_{Ho} < \lambda_{Tb} < \lambda_{Dy}$, $I_{Nd} < I_{Dy} < I_Y < I_{Tb} < I_{Ho} < I_{La} < I_{Tm} < I_{Er}$. Inset illustrated the excitation peak of $SrAl_2O_4$: Eu^{2+}, Dy^{3+} phosphor located at 365 nm corresponding to the transition of Eu^{2+} ion from $4f^7 \rightarrow 4f^65d$. Meanwhile, it is well known that the excited $4f^65d$ configurations of Eu^{2+} ions are extremely sensitive to the change in the lattice environment contrast to the shielded $4f^7$ ground configurations, and the 5d electron may couple strongly with the lattice [13]. Therefore, the mixed states of 4f and 5d would be influenced strongly by the crystal field [14]. Since the crystal field around Eu^{2+} ion was different with the varied co-activator ions doping, which induced the different splitting extent of 5d electrons energy levels [15] and caused the emission wavelength to exhibit red shift in

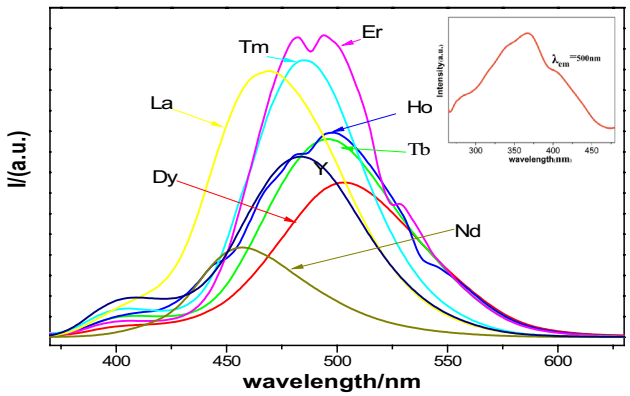

Fig. 3 The fluorescence emission spectra of $SrAl_2O_4$: Eu^{2+}, RE^{3+} phosphors (RE = Dy, Tb, Ho, Tm, Er, La, Nd, Y). Inset illustrates the excitation spectra of $SrAl_2O_4$: Eu^{2+}, Dy^{3+} phosphor

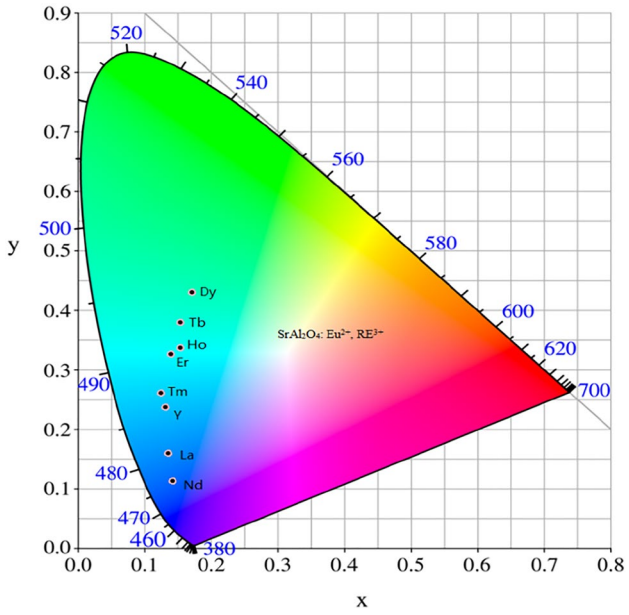

Fig. 4 CIE chromaticity diagram of $SrAl_2O_4$: Eu^{2+}, RE^{3+} phosphors (RE = Dy, Tb, Ho, Tm, Er, La, Nd, Y)

different degrees. Moreover, the depths of electron traps were different under varied co-activator doping, which caused diverse fluorescence intensity. The experiment results were different from previous conclusions that the species of co-activators had no effect on the emission wavelength. Also, we could see clearly that two strong emission peaks appeared at 482 nm and 499 nm after Er^{3+} doping, which caused the emission wavelength range was widened and thus forming a broad emission. The possible reason was that Er^{3+} occupied two different sites in the matrix lattice and thus two kinds of emission centers were formed [16]. Consequently, products doped by co-activator Er^{3+} had a better performance.

The Commission International de I'E clairage (CIE) chromaticity diagram of the $SrAl_2O_4$: Eu^{2+}, RE^{3+} (Dy, Tb, Ho, Tm, Er, La, Nd, Y) phosphors was depicted in Fig. 4, the color coordinate were summarized in Table 1 [17]. It could be seen that the luminescence color was blue when La and Nd were employed as co-activators, and was blue-green while Er^{3+}, Y^{3+}, Tm^{3+}, Tb^{3+}, Ho^{3+} and Dy^{3+} were employed as co-activators. The result was further evidence that the co-activators species had vital effects on emission wavelength of phosphors.

3.2.2 Fluorescence spectrum analysis of $SrAl_2O_4$: Eu^{2+}, Dy^{3+}, M^{2+} phosphors

The fluorescence spectra of $SrAl_2O_4$: Eu^{2+}, Dy^{3+}, M^{2+} (M = Mn^{2+}, Ni^{2+}, Mg^{2+}, Cu^{2+}, Zn^{2+}) phosphors under different doping concentration were shown in Fig. 5. It could be seen that the fluorescence emission peaks positions of products showed a slight blue shift when doped with Mn^{2+}, Ni^{2+}, Cu^{2+}, Zn^{2+} ions, but were not changed when doped with Mg^{2+} ion, which indicated the crystal field around emission center Eu^{2+} ion was changed under the doping of different transition metal ions. Meanwhile, the dependence of fluorescence emission intensity on doping concentration of transition metal ions was shown in Fig. 5 and the photographs of $SrAl_2O_4$: Eu^{2+}, Dy^{3+}, Mn^{2+} phosphors were showed in the Inset. It could be seen that the fluorescence emission intensity decreased with the increment of the doping concentration of transition metal ions. It might be because the crystal field around the emission center (Eu^{2+}) was changed after transition metal ions doping, which caused the splitting extent of 5d electrons energy levels to be changed, and thus the emission peaks positions of Eu^{2+} were changed slightly. Moreover, some Sr^{2+} sites would be replaced by transition metal ions when they were doped into matrix under the optimal concentration of co-activator (Dy^{3+}) providing electron traps, but the radius of them (Mn^{2+} (67 pm), Ni^{2+} (69 pm), Mg^{2+} (72 pm), Cu^{2+} (73 pm), Zn^{2+} (76 pm)) and Sr^{2+} (118 pm) differ considerably, which

Table 1 CIE parameters of $SrAl_2O_4$: Eu^{2+}, RE^{3+} (Dy, Tb, Ho, Tm, Er, La, Nd, Y) phosphors

Products	CIE coordinate (*x*, *y*)
$SrAl_2O_4$: Eu^{2+}, Dy^{3+}	(0.1713,0.4308)
$SrAl_2O_4$: Eu^{2+}, Tb^{3+}	(0.1534,0.3794)
$SrAl_2O_4$: Eu^{2+}, Ho^{3+}	(0.1534,0.3377)
$SrAl_2O_4$: Eu^{2+}, Tm^{3+}	(0.1239,0.2614)
$SrAl_2O_4$: Eu^{2+}, Er^{3+}	(0.1382,0.3264)
$SrAl_2O_4$: Eu^{2+}, La^{3+}	(0.1364,0.1605)
$SrAl_2O_4$: Eu^{2+}, Nd^{3+}	(0.141,0.1139)
$SrAl_2O_4$: Eu^{2+}, Y^{3+}	(0.1308,0.2375)

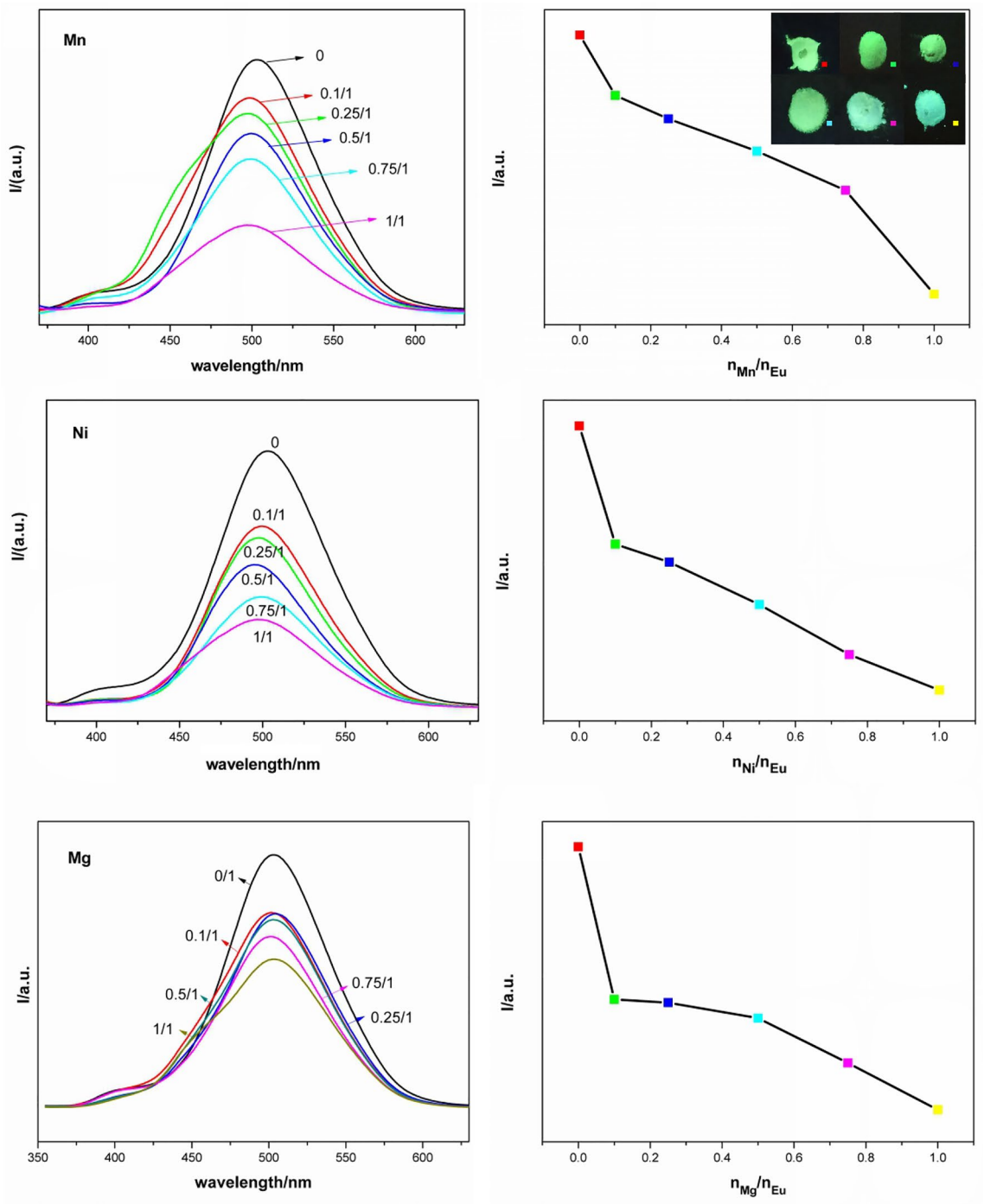

Fig. 5 The fluorescence emission spectra of $SrAl_2O_4$: Eu^{2+}, Dy^{3+}, M^{2+} phosphors (M = Mn, Ni, Mg, Cu, Zn) and the dependence of fluorescence emission intensity on transition metal ions doping concentration. Inset illustrates the photograph of $SrAl_2O_4$: Eu^{2+}, Dy^{3+}, Mn^{2+} phosphors (n_{Mn}/n_{Eu} = 0, 0.1, 0.25, 0.5, 0.75, 1) under UV lamp

might form the impurity traps that caused trap concentration to be too large [18]. When the excitation was stopped, a large number of electrons were released and then transitioned to excited state, which caused the concentration of the excited state emission center (Eu^{2+}) to be excessive, and the probability of collisions and energy transfer between adjacent Eu^{2+} ions to increase, thus the concentration quenching to be happen [19] and the emission intensity was reduced. Wherein, it was showed that the variations of emission intensity for $SrAl_2O_4$: Eu^{2+}, Dy^{3+}, M^{2+} (M = Mg^{2+}, Zn^{2+}) were not very clear. The possible reason for Mg^{2+} ion doping was that the atomic mass of Mg^{2+} ion (24.31) is much smaller

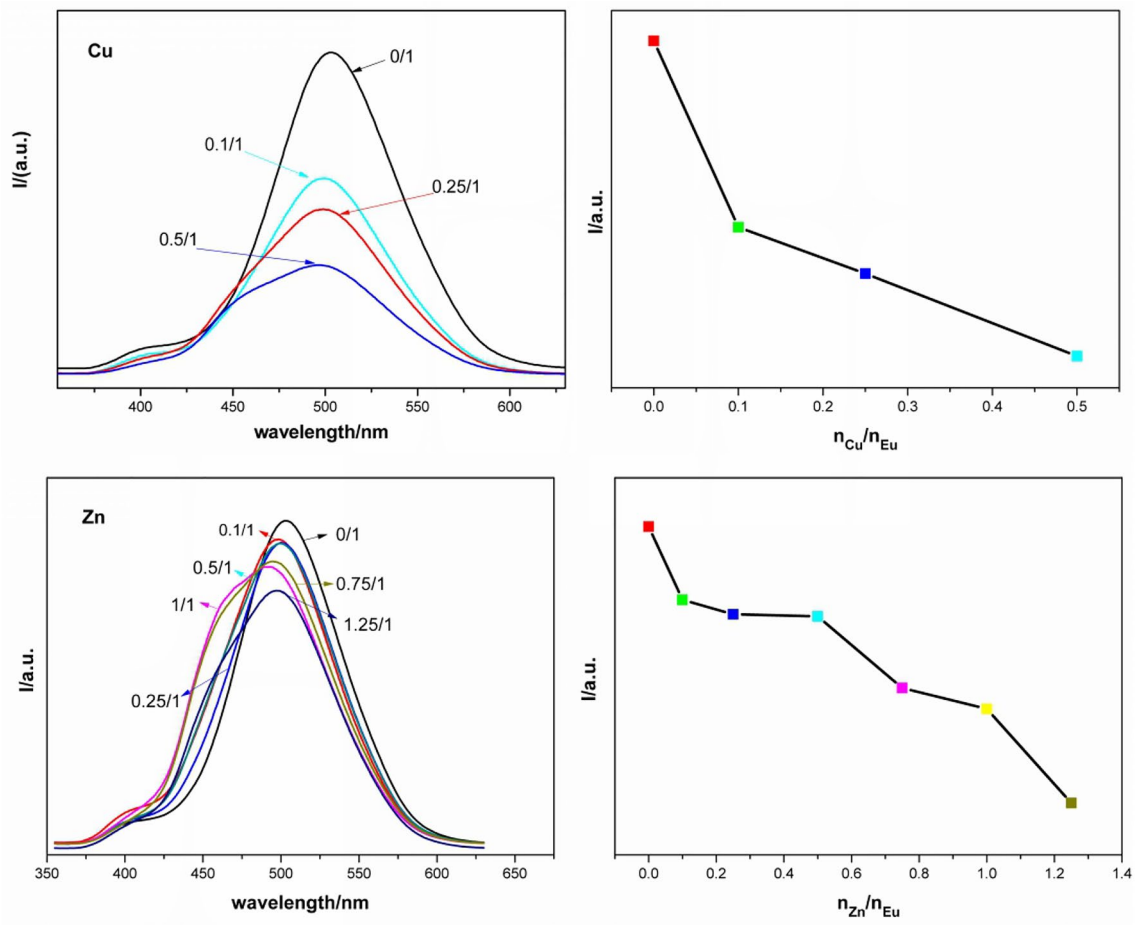

Fig. 5 (continued)

than Sr^{2+} ion (87.62), which caused the crystal phase transition of main crystal phase toward hybrid phase, and thus a little effect on the emission intensity. For Zn^{2+} ion doping, it might be because its radius and atomic mass are nearest to those of Sr^{2+} ion, which caused fewer trap concentration and then the less concentration quenching [20], further the indistinct decrease of emission intensity.

3.3 SEM and EDX analysis

The morphology analysis and elements compositions of the products (take $SrAl_2O_4$: Eu^{2+}, Dy^{3+} as an example) were shown in Fig. 6. It could be observed directly that the resultant crystal particles exhibited a uniform distribution and regular hexagon flake-like morphology with a width of ~ 500 nm and a thickness of ~ 70 nm, which showed good crystallization of products. Meanwhile, the elements compositions of the $SrAl_2O_4$: Eu^{2+}, Dy^{3+} phosphors were illustrated by EDX mapping, and thus the presence of strontium (Sr), aluminum (Al), oxygen (O), europium (Eu) and dysprosium (Dy) were confirmed.

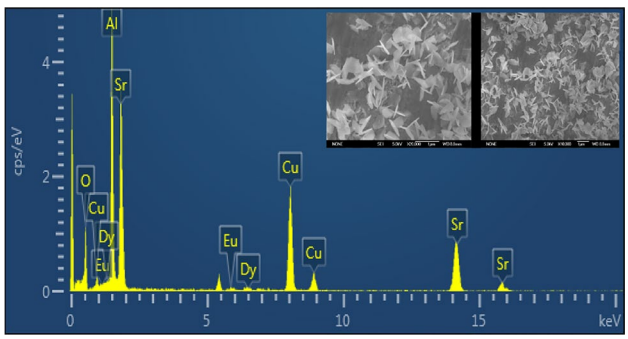

Fig. 6 The SEM images and EDX spectroscopy of $SrAl_2O_4$: Eu^{2+}, Dy^{3+} phosphors

4 Conclusion

The $SrAl_2O_4$: Eu^{2+} phosphors doped with different co-activators and transition metal ions were synthesized by hydrothermal and co-precipitation methods, and the

products were explored by means of X-ray diffraction (XRD), fluorescence spectrometer and SEM.

XRD patterns showed $SrAl_2O_4$: Eu^{2+}, RE^{3+} phosphor presented different diffraction peak position and the diffraction peak intensity after doped by different co-activator ions. Interestingly, the peak positions were unaltered after doped by transition metal ions (Mn^{2+}, Ni^{2+}, Mg^{2+}, Cu^{2+}, Zn^{2+}), while the peak intensity of crystal phase $Sr_4Al_{14}O_{25}$ was enhanced after doped by cations (Mn^{2+}, Ni^{2+}, Cu^{2+}, Zn^{2+}), which indicated the doping of cations (Mn^{2+}, Ni^{2+}, Cu^{2+}, Zn^{2+}) could facilitate the crystal phase transition from $SrAl_2O_4$ toward $Sr_4Al_{14}O_{25}$.

The fluorescence analysis results indicated that the species of co-activator ions had a significant impact on the luminescence properties of products. The sequence of emission wavelength and emission intensity was as follows: $\lambda_{Nd} < \lambda_{La} < \lambda_{Er} < \lambda_{Y} < \lambda_{Tm} < \lambda_{Tb} < \lambda_{Ho} < \lambda_{Dy}$, $I_{Nd} < I_{Dy} < I_{Y} < I_{Tb} < I_{Ho} < I_{La} < I_{Tm} < I_{Er}$. The result is a revision about the previous conclusions: co-activators species have no any effects on emission wavelength. Moreover, the luminescent intensities of products were reduced after being doped by transition metal ions under the optimal concentration of co-activator. However, the emission wavelength positions were not changed after doped by transition metal ions (Mg^{2+}) compared to a blue shift after doped by cations (Mn^{2+}, Ni^{2+},Cu^{2+}, Zn^{2+}). The crystal particles of $SrAl_2O_4$: Eu^{2+}, Dy^{3+} presented regular hexagon flake-like morphology with a width of ~ 500 nm and a thickness of ~ 70 nm. The title products could be applied in the safety indicators, emergency lighting danger signals, automobiles, solar cells, etc.

Acknowledgements The authors are grateful for the financial support of the National Natural Science Foundation of China (Nos. J1103312, J1210040 and 21341010), the Natural Science Foundation of Hunan Province (No. 11JJ5005), Hunan provincial Science & Technology Department (No. 2016SK2064), Changsha Science & Technology Bureau (Nos. kq1701164 and kq1701029), the Innovative Research Team in University (No. IRT1238), and China Outstanding Engineer Training Plan for Students of Chemical Engineering & Technology in Hunan University (MOE-No.2011-40). We also thank Dr. William Hickey, the U.S. professor of HRM, for the English editing on this paper.

References

1. S. Bishnoi, B. Rajesh, G. Swati, V. Vikesh Jaiswal, M. Sahu, P. Singh, D. Haranath, Mater. Today Proc. **5**, 610 (2018)
2. C. Xu, J. Nie, Z. Xu, X. Liu, J. Qiu, Mater. Lett. **225**, 97 (2018)
3. A.S. Lysenkov, Y.F. Kargin, D.D. Titov, N.V. Petrakova, S.N. Ivicheva, A.I. Zakharov, N.A. Popova, V.V. Zakorzhevskii, I.P. Borovinskaya, I.S. Melnikova, IOP Conf. Ser. Mater. Sci. Eng. **347**, 012040 (2018)
4. W.J. Lai, K.C. Cheng, Fibers Polym. **19**, 22 (2018)
5. N.A.S. Rabaoui, K.O. Rabia, Appl. Phys. A **124**, 1 (2018)
6. K.O.A. Alyamani, L. El Mir, Appl. Phys. A **124**, 1 (2018)
7. T. Aitasalo, A. Durygin, J. Hölsä, M. Lastusaari, J. Niittykoski, A. Suchocki, J. Alloys Compd. **380**, 4 (2004)
8. A. Salehabadi, M. Salavati-Niasari, F. Sarrami, A. Karton, Renew. Energy **114**, 1419 (2017)
9. W. Xie, J. Quan, H. Wu, L. Shao, C. Zou, J. Zhang, X. Shi, Y. Wang, J. Alloys Compd. **514**, 97 (2012)
10. C.C. Ã, W. Li, X. Huang, Z. Wang, X. Chen, X. Qian, R. Guo, Y. Ding, D. Mao, J. Lumin. **130**, 347 (2010)
11. W. Jia, H. Yuan, L. Lu, H. Liu, W.M. Yen, J. Lumin. **76–77**, 424 (1998)
12. X. Hu, H. Yang, T. Guo, D. Shu, W. Shan, G. Li, D. Guo, Ceram. Int. **44**, 7535 (2018)
13. Z. Xue, S. Deng, Y. Liu, B. Lei, Y. Xiao, M. Zheng, J. Rare Earths **31**, 241 (2013)
14. W. Shan, L. Wu, N. Tao, Y. Chen, D. Guo, Ceram. Int. **41**, 15034 (2015)
15. P. Du, E.J. Kim, J.S. Yu, Curr. Appl. Phys. **18**, 310 (2018)
16. R. Zhang, G. Han, L. Zhang, B. Yang, Mater. Chem. Phys. **113**, 255 (2009)
17. P. Du, J.S. Yu, J. Alloys Compd. **653**, 468 (2015)
18. F. Clabau, X. Rocquefelte, S. Jobic, P. Deniard, M.H. Whangbo, A. Garcia, T. Le Mercier, Chem. Mater. **17**, 3904 (2005)
19. H. Du, W. Shan, L. Wang, D. Xu, H. Yin, Y. Chen, D. Guo, J. Lumin. **176**, 272 (2016)
20. D.S. Kshatri, A. Khare, P. Jha, Opt. Int. J. Light Electron. Opt. **124**, 2974 (2013)